Effects of gravity on the acceleration and pair statistics of inertial particles in homogeneous isotropic turbulence

H. Parishani, O. Ayala, B. Rosa, L.-P. Wang, and W. W. Grabowski

Citation: Physics of Fluids (1994-present) **27**, 033304 (2015); doi: 10.1063/1.4915121
View online: http://dx.doi.org/10.1063/1.4915121
View Table of Contents: http://scitation.aip.org/content/aip/journal/pof2/27/3?ver=pdfcov
Published by the AIP Publishing

PHYSICS OF FLUIDS **27**, 033304 (2015)

Effects of gravity on the acceleration and pair statistics of inertial particles in homogeneous isotropic turbulence

H. Parishani,[1,2] O. Ayala,[3] B. Rosa,[4] L.-P. Wang,[2,5,a)] and W. W. Grabowski[6]
[1]*Department of Earth System Science, University of California, Irvine, California 92697-3100, USA*
[2]*Department of Mechanical Engineering, University of Delaware, Newark, Delaware 19716-3140, USA*
[3]*Department of Engineering Technology, Old Dominion University, 214 Kaufman Hall, Norfolk, Virginia 23529, USA*
[4]*Institute of Meteorology and Water Management-National Research Institute, 61 Podlesna Street, 01-673 Warsaw, Poland*
[5]*The State Key Laboratory of Coal Combustion, Huazhong University of Science and Technology, Wuhan 430074, People's Republic of China*
[6]*Mesoscale and Microscale Meteorology Division, National Center for Atmospheric Research, P.O. Box 3000, Boulder, Colarado 80307, USA*

(Received 7 May 2014; accepted 27 February 2015; published online 19 March 2015)

Within the context of heavy particles suspended in a turbulent airflow, we study the effects of gravity on acceleration statistics and radial relative velocity (RRV) of inertial particles. The turbulent flow is simulated by direct numerical simulation (DNS) on a 256^3 grid and the dynamics of $O(10^6)$ inertial particles by the point-particle approach. For particles/droplets with radius from 10 to 60 μm, we found that the gravity plays an important role in particle acceleration statistics: (a) a peak value of particle acceleration variance appears in both the horizontal and vertical directions at a particle Stokes number of about 1.2, at which the particle horizontal acceleration clearly exceeds the fluid-element acceleration; (b) gravity constantly disrupts quasi-equilibrium of a droplet's response to local turbulent motion and amplifies extreme acceleration events both in the vertical and horizontal directions and thus effectively reduces the inertial filtering mechanism. By decomposing the RRV of the particles into three parts: (1) differential sedimentation, (2) local flow shear, and (3) particle differential acceleration, we evaluate and compare their separate contributions. For monodisperse particles, we show that the presence of gravity does not have a significant effect on the shear term. On the other hand, gravity suppresses the probability distribution function (pdf) tails of the differential acceleration term due to a lower particle-eddy interaction time in presence of gravity. For bidisperse cases, we find that gravity can decrease the shear term slightly by dispersing particles into vortices where fluid shear is relatively low. The differential acceleration term is found to be positively correlated with the gravity term, and this correlation is stronger when the difference in colliding particle radii becomes smaller. Finally, a theory is developed to explain the effects of gravity and turbulence on the horizontal and vertical acceleration variances of inertial particles at small Stokes numbers, showing analytically that gravity affects particle acceleration variance both in horizontal and vertical directions, resulting in an increase in particle acceleration variance in both directions. Furthermore, the effect of gravity on the horizontal acceleration variance is predicted to be stronger than that in the vertical direction, in agreement with our DNS results. © *2015 AIP Publishing LLC.* [http://dx.doi.org/10.1063/1.4915121]

a)Electronic mail: lwang@udel.edu

I. INTRODUCTION

Understanding the dynamics of inertial particles in a turbulent flow is of importance to a wide range of applications in astrophysics (proto-planetary dust), environmental sciences (sediment transport, sea spray, rain development), and industrial processes (spray nozzles, fluidized bed reactors). Acceleration statistics of inertial particles in a turbulent flow is a natural extension to the Lagrangian description of fluid elements, and it is relevant to the dynamics, transport, dispersion, and, collision of dust particles and small droplets suspended in the atmosphere. In this paper, we systematically study the effects of gravity on particle acceleration statistics and particle-particle radial relative velocity (RRV).

Acceleration statistics of inertial particles have been studied in recent years to better understand the nature of the forces acting on the particles and the effects of particle inertia and gravity on particle dynamics. The topic has received increasing attention in the recent years due to the emergence of experimental tools and methods to measure particle acceleration. Ayyalasomayajula *et al.*[1] measured acceleration of water droplets in a grid generated turbulence at Taylor microscale Reynolds number of $R_\lambda = 250$. They showed that the acceleration probability distribution function (pdf) of inertial particles has narrower tails than those of a tracer. Their measurements also indicate that particle acceleration variance decreases with particle Stokes number (St). Volk *et al.*[2] performed laboratory experiments at $R_\lambda = 850$ and compared particle acceleration statistics with direct numerical simulation (DNS) results at $R_\lambda = 185$. They observed a qualitative agreement of the pdf shape and the acceleration autocorrelation function between laboratory experiments and DNS. The quantitative differences in their results arise mainly due to the fact that their DNS consisted of point-particles at a much lower flow Reynolds number ($R_\lambda = 185$) compared to their experiments where $R_\lambda = 850$.

Qureshi *et al.*[3] studied acceleration statistics of finite-size inertial particles and found that particle size and density variations only affect the acceleration variance leaving the acceleration pdf unchanged. On the other hand, Calzavarini *et al.*[4] showed that point-particles with inertia and Stokes drag do not fully capture the particle acceleration. They compared DNS and experimental data and showed that Faxen corrections are needed to yield a more accurate acceleration statistics. For higher Reynolds numbers, Volk *et al.*[5] performed an experimental study of particle acceleration in Von-Karman turbulence for large neutrally buoyant particles ($2a/\eta \geq 1$, where a and η are particle radius and Kolmogorov length scale, respectively). Being able to generate flows at $R_\lambda = 590$ and 1050, they found that particle acceleration variance scales with $(2a/\eta)^{-2/3}$. They also showed that the tails of particle acceleration pdf narrow with increasing particle size. However, their acceleration measurements are performed using only one spatial component of velocity and may not be representative of the particle acceleration vector in presence of gravity. Prakash *et al.*[6] carried out laboratory experiments to study acceleration of bubbles, where the particle-to-fluid density ratio is nearly zero, in the size range $2a/\eta = 7$–12. For the two Reynolds numbers $R_\lambda = 145$ and 230, they found that gravity increases the acceleration variance and reduces the acceleration intermittency in the vertical direction. They were able to cross validate their experiments with DNS when the Faxen corrections were included. This implies that the finite-size effect and gravity are coupled together to alter the bubble acceleration.

On the numerical computation front, acceleration statistics of inertial particles have been studied in the pioneering work of Bec *et al.*[7] using DNS of turbulence. They demonstrated two important mechanisms governing the particle acceleration. First, they argued that the preferential concentration of inertial particles in low-vorticity regions of the flow causes a *biased sampling* of local fluid acceleration at small to moderate particle Stokes numbers. Second, they showed that at larger St, particle response time (τ_p) acts as a low-pass filter inducing a *filtering effect* to particle acceleration. They noted that these two effects take place simultaneously and both are related to the particle inertia. In a more recent DNS study, Salazar and Collins[8] further demonstrated the biased filtering effect which was previously introduced by Ayyalasomayajula *et al.*[1] Using conditional statistics and pdf tools, Salazar and Collins[8] found that stronger acceleration events are filtered more intensely by particle inertia than weaker accelerations. While different effects of particle inertia (sampling and filtering) cannot be decoupled in experimental studies, the biased sampling effect and the filtering effect can be artificially decoupled in numerical simulations by using altered equations of motion for the particles, a technique originally introduced by Bec *et al.*[7]

Furthermore, using a DNS of turbulent channel flow, Lavezzo *et al.*[9] studied the particle acceleration in near-wall region for a flow with shear Reynolds number $R_\tau = 300$ and particles with Stokes numbers $St = 0.87, 1.76$, and 11.8. Consistent with the experiments of Gerashchenko *et al.*,[10] Lavezzo *et al.*[9] found that the particle rms acceleration in the stream-wise direction increases with Stokes number in the near-wall regions. This behavior is in fact the opposite of the trend observed for particles in isotropic turbulence. They also found that the presence of gravity significantly increases the stream-wise particle rms acceleration in the near-wall regions. They argued that this increase might be related to the strong coupling of gravity and shear in the near-wall region in such a way that gravity pulls the particles to near-wall regions whereby decelerating them due to higher fluid shear. They demonstrated that the effect of gravity on particle acceleration is the most profound for the largest particles ($St = 11.8$).

Effect of gravity on the collision of monodisperse droplets in homogeneous isotropic turbulence is studied by Onishi *et al.*[11] Through DNS with grid resolutions up to 96^3, they showed that gravity decreases the droplet-eddy interaction time leading to a weaker relative velocity between the droplets. Based on DNS results, they formulated a model to estimate the impact of gravity on the collision kernel of inertial particles. In a more recent DNS study, Park and Lee[12] showed that gravity can cause vertical-strip clustering for large particles ($St > 1$). They showed that this type of preferential concentration exists provided there is a strong sedimentation through turbulence. Their DNS data confirm that heavy particles settling under strong gravity are more exposed to regions with converging fluid motion in the horizontal plane and thus are able to form clustered strips in the vertical direction.

In many natural phenomena, the gravity plays a very important role and its effect on particle acceleration must be understood. The effect of gravity has received attention only in recent experimental studies (Ayyalasomayajula *et al.*,[1] Volk *et al.*,[2] Volk *et al.*,[5] and Prakash *et al.*[6]), and very few numerical investigations (e.g., in Mazzitelli and Lohse[13] for bubbles and fluid particles, Onishi *et al.*[11] and Park and Lee[12]) have taken it into account.

So far, most studies focus on the effect of turbulent Reynolds number and particle Stokes number on acceleration of inertial particles. Furthermore, previous studies concern only single-particle acceleration statistics. Two-particle or differential acceleration statistics are important in formulating the radial relative velocity between two inertial particles,[14] which have not yet been studied. Recently, Grabowski and Wang[14] showed that when the Stokes drag, particle inertia, and gravity are considered together and the particle size is smaller than the flow Kolmogorov scale, the RRV consists of three contributions: (1) differential sedimentation (w_g), (2) local flow shear (w_s), and (3) particle differential acceleration (w_a). Gravity undoubtedly affects the first as well as the third contribution. Using scaling estimates, they argued that the net effect of turbulence on the RRV of inertial droplets is mostly due to the local acceleration effect. In this paper, we follow their decomposition to gain more insight into differential acceleration and consequently radial relative velocity of inertial particles.

II. THE NUMERICAL METHOD

We consider a dilute suspension (mass loading $\sim O(10^{-3})$) of non-deformable droplets in a background turbulent air flow. The dilute droplet concentration allows a one-way coupling between the dispersed phase and the air flow. Furthermore, in this study, we employ a point particle approach under the assumption that the particle diameter is much smaller than the flow Kolmogorov scale. The fluid velocity $\mathbf{U}(\mathbf{x},t)$ is obtained by a pseudo-spectral method in a periodic domain by solving the Navier-Stokes equation:

$$\frac{\partial \mathbf{U}}{\partial t} = \mathbf{U} \times \omega - \nabla \left(\frac{P}{\rho} + \frac{1}{2}\mathbf{U}^2 \right) + \nu \nabla^2 \mathbf{U} + \mathbf{f}(\mathbf{x},t), \tag{1}$$

for an incompressible fluid satisfying the continuity equation,

$$\nabla \cdot \mathbf{U}(\mathbf{x},t) = 0. \tag{2}$$

Here, $\omega \equiv \nabla \times \mathbf{U}$ is the vorticity, P is the pressure, ρ is fluid density, and ν is fluid kinematic viscosity (of air in our simulation). The domain is a cube of dimension of 2^n in each direction and is discretized uniformly using N^3 grid points, with periodic boundary conditions. Here, N is the number of grid points in each direction and takes the values of 2^n, n being a positive integer. The approach is therefore a DNS of turbulence. For each given time step, Eq. (1) is integrated in the Fourier space to yield the time-dependent three-dimensional fluid velocity $\mathbf{U}(\mathbf{x},t)$. An inverse Fourier transform yields the turbulent fluid velocities at the grid points in the physical space.

A stationary turbulence is maintained by the forcing term $\mathbf{f}(\mathbf{x},t)$ which is nonzero only for a few low-wavenumber modes ($|k| < \sqrt{8}$) in the Fourier space. We implemented two forcing methods allowing us to study the sensitivity of results on the forcing method. The two forcing methods are as follows.

1. Deterministic forcing of Sullivan *et al.*:[15] In this type of forcing, flow could be initialized from any random field of $\mathbf{U}(\mathbf{x},t)$. For each of the first two wavenumber shells ($|k| = 1$ and 2), the Fourier coefficients of the modes within a shell are augmented by a constant factor at the end of the time step so that a prescribed energy level for the shell is restored. The prescribed energy levels are made consistent with the $k^{-5/3}$ spectrum.
2. Stochastic forcing of Eswaran and Pope:[16] If this forcing is used, we develop the flow from rest. The forcing term $\mathbf{f}(\mathbf{x},t)$ then applies force in the Fourier space to modes with low wavenumbers ($|k| < \sqrt{8}$). In this method, for each Fourier mode, 6 independent Uhlenbeck-Ornstein processes are combined to specify the complex Fourier coefficient of the forcing term, $a_f(\mathbf{x},t)$.

The details of the large-scale forcing may affect the simulated statistics of inertial particles for two general reasons. First, the large-scale forcing could affect the small-scale structures through triadic interactions (e.g., Yeung *et al.*[17]). Second, finite inertia and sedimentation of heavy particles imply that a heavy particle responds to a range of scales in the flow. Therefore, if the DNS flow Reynolds number is limited (so the scales of simulated flow are limited), large-scale fluid velocity and acceleration contributed by the forcing can affect the particle dynamics directly. Rosa *et al.*[18,19] showed that the quantitative collision statistics of particles with large response time could depend on the details of a large-scale forcing scheme.

We first evolve the flow (without droplets) from $t = 0$ up to at least $t = 18T_e$ (T_e is the large-eddy turnover time) to ensure that the flow is statistically stationary. This eliminates any effect of initial flow condition on the statistics and dynamics of the resulting stationary homogeneous and isotropic turbulence. Inertial particles are then introduced into the flow. The fluid velocity at the location of the kth droplet of radius $a^{(k)}$, denoted by $\mathbf{U}(\mathbf{Y}^{(k)}(t),t)$, is interpolated from the grid using the 6-point Lagrangian interpolation in each spatial direction, where $\mathbf{Y}^{(k)}(t)$ is the location of the droplet. The velocity of the kth droplet will be denoted by $\mathbf{V}^{(k)}(t)$. Droplets are advanced by solving their equation of motion

$$\frac{d\mathbf{V}^{(k)}(t)}{dt} = -\frac{\mathbf{V}^{(k)}(t) - \mathbf{U}(\mathbf{Y}^{(k)}(t),t)}{\tau_p^{(k)}} + \mathbf{g}, \tag{3}$$

$$\frac{d\mathbf{Y}^{(k)}(t)}{dt} = \mathbf{V}^{(k)}(t), \tag{4}$$

where $\tau_p^{(k)} = \frac{2\rho_p (a^{(k)})^2}{9\mu}$ is the Stokes inertial response time of the kth droplet and $\mathbf{g}$ is the gravitational acceleration ($|\mathbf{g}| = 9.8\ \mathrm{m/s^2}$). ρ_p is particle/droplet density and μ is the fluid viscosity. In this study, the particle diameter is smaller than the Kolmogorov length of the turbulence, and therefore the finite-size effects are not important here.

Particle acceleration is computed using the RHS of (3) and is averaged over different particles and time. In Eq. (3), $\mathbf{g}$ is turned on/off to study the effect of gravitational acceleration. The gravitational force (if present) is considered to be in the third (vertical) direction. For the current study, we have used a highly scalable code based on 2D domain decomposition. Our parallel implementation is based on the Message Passing Interface (MPI), with the domain decomposition strategy previously adopted for the efficient MPI implementation of Fast Fourier Transform (FFT) in the pseudo-spectral simulation of fluid turbulence.[20] We measured the wall clock time of the code under

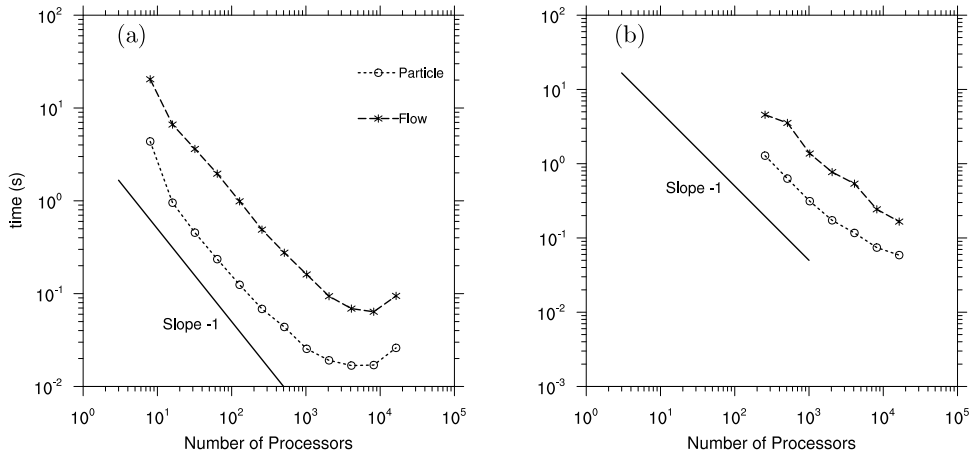

FIG. 1. Measured wall-clock time for two settings: (a) 512^3, 45 μm-60 μm, 730 000 particles ($LWC \sim 2.2$ g/m^3), (b) 1024^3, 20 μm-30 μm, 16 500 000 particles ($LWC \sim 1.0$ g/m^3). Measurements are performed on Stampede at Texas Advanced Computing Center (TACC).

different simulation conditions. In Figure 1, we show the measured wall-clock times for different number of processors and for two grid resolutions. The data points for the number of processors cover 3 decades. A line of slope −1 is plotted to serve as reference for ideal scalability. The execution time scales with the number of processors almost linearly before the scalability saturates due to excessive communication latency. More details of this scalable implementation could be found in Ayala *et al.*[21] and Torres *et al.*[22]

III. RESULTS

We report DNS results obtained using a 256^3 resolution for 6 particle radii at 10, 20, 30, 40, 50, and 60 μm (St = 0.06, 0.25, 0.57, 1.01, 1.59, and 2.28, respectively) in the context of cloud physics. At this resolution, we achieved $R_\lambda = 143$ for the deterministic forcing and $R_\lambda = 119$ for the stochastic forcing. The data have been gathered and post-processed from 2000 snapshots of $O(10^6)$ particles over a time period of $\sim 48T_e$. The magnitude of the forcing ensures that the mean dissipation rate of kinetic energy is held at $\epsilon = 400$ cm^2/s^3. The details of flow properties are tabulated in Table I. It should be noted that while the flow statistics under the two forcing schemes differ significantly in DNS units due to different DNS settings, they are comparable when converted into physical units using the above physical dissipation rate and the air viscosity. In this study, $a_\eta/|\mathbf{g}| \sim 0.14$ and therefore the average fluid acceleration is about one order of magnitude smaller than the gravitational acceleration.

In our simulations, the ratio of integral length scale L_f to the domain size (2π in DNS units) is 0.23 and 0.15 for deterministic and stochastic forcing, respectively. Physically, as a minimum, the two-point correlations of the solution are required to decay nearly to zero within half the domain to ensure proper statistical representation of the large scales.[23] Past experience has indicated that if this ratio is less than 0.3 (e.g., Eswaran and Pope[16]), the statistics of fluid turbulence does not depend on the imposed periodicity. In our simulations, this condition is satisfied.

A. Particle acceleration statistics

In Figure 2 the pdf of acceleration is plotted for non-sedimenting particles (i.e., set **g** to zero in Eq. (3)) and compared with the previously published data of Bec *et al.*[7] who used a deterministic forcing to drive the turbulent flow. Two particle Stokes numbers $St = 1.01$ and 2.3 are considered. The results are in reasonable agreement and show that the pdf values for the larger Stokes number are smaller in the tail due to the inertial filtering and biased sampling effects.[8] The flow Reynolds

TABLE I. Flow parameters in both DNS and physical units. From top to bottom are: viscosity ν, energy dissipation rate ϵ, time step size δt, rms velocity u', eddy turn-over time T_e, Kolmogorov velocity v_k, Kolmogorov timescale τ_k, Kolmogorov length scale η, fluid acceleration at Kolmogorov scale a_η, integral length scale L_f, Taylor scale Reynolds number R_λ, and the spatial resolution parameter $k_{max}\eta$.

	Deterministic		Stochastic	
	DNS	Physical units	DNS	Physical units
ν	0.002	0.17 cm^2/s	0.0375	0.17 cm^2/s
ϵ	0.2134	400 cm^2/s^3	3563.4	400 cm^2/s^3
δt	0.001	0.000 212 s	0.000 041	0.000 259 s
u'	0.8729	17.5 cm/s	18.79	15.83 cm/s
T_e	3.614	0.768 s	0.0952	0.601 s
v_k	0.143	2.87 cm/s	3.405	2.87 cm/s
τ_k	0.096 94	0.0206 s	0.003 26	0.0206 s
η	0.0139	0.0592 cm	0.0111	0.0592 cm
a_η	1.475	139.32 cm/s^2	1044.47	139.32 cm/s^2
L_f	1.4328	6.1022 cm	0.9603	5.1216 cm
R_λ	143	143	119	119
$k_{\max}\eta$	1.67	...	1.39	...

number R_λ was 185 in Bec *et al.*,[7] higher than $R_\lambda = 143$ in our simulations which explains why the tails in Bec *et al.*[7] are slightly more extended.

The pdfs of particle acceleration are shown in Figure 3 comparing the results from the two forcing schemes in our simulations. A close-up is plotted in Figure 3(b) for more detailed comparison. The figures show that the two forcing schemes yield approximately the same pdf for the normalized acceleration, although we observe some differences in the rms values of acceleration (to be discussed next).

To validate further, we compare in Figure 4(a) the results of normalized rms acceleration against those of Bec *et al.*[7] and Salazar and Collins[8] for non-sedimenting particles. A deterministic forcing scheme was used in both Bec *et al.*[7] and Salazar and Collins.[8] Acceleration values are

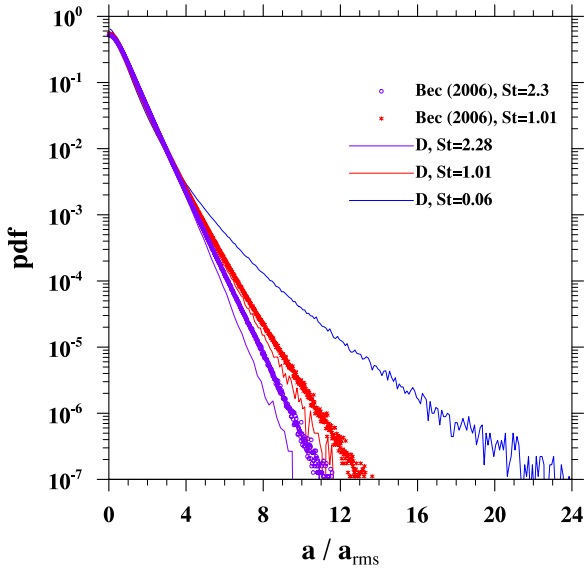

FIG. 2. The pdfs of normalized particle acceleration are compared against the results of Bec *et al.*[7] Legend: D denotes the deterministic forcing.

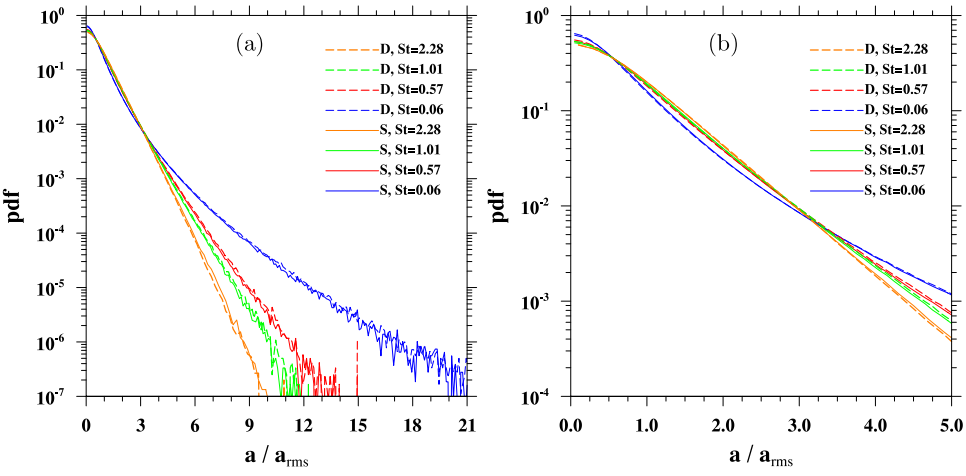

FIG. 3. The pdfs of normalized particle acceleration obtained using two different forcing methods. (b) is a zoom-in of (a). Legend: D denotes the deterministic forcing; S is for the stochastic forcing.

normalized by fluid element acceleration, expressed as $a_\eta a_0$, where $a_\eta = (\epsilon^3/\nu)^{1/4}$ represents the level of the small scale fluid acceleration and $a_0 = 2.5R_\lambda^{0.25} + 0.08R_\lambda^{0.11}$ is an empirical fitting correlation taken from Hill[24] to account for the finite R_λ differences in the data sets. The rms acceleration from our study collapses almost identically on the published data. We confirm that there is a sharp initial decrease in particle rms acceleration with increasing St when $St < 1$. The rate of decrease is smaller for larger particle Stokes numbers. Alternative empirical correlations are available for a_0 at low flow Reynolds number, for instance, in Sawford *et al.*[25] These alternative correlations, however, were found to yield almost the same plots in Figure 4(a).

Figure 4(a) also shows that our stochastic forcing yields a slightly higher rms acceleration than the results from our deterministic forcing. The smaller size of the flow vortical structures under the stochastic forcing could contribute to this difference. The results together show that the details of the large-scale forcing could slightly affect the magnitude of the rms acceleration, but it is not significant when compared to the change due to the effect of St.

Now, we focus on the effect of gravity on particle acceleration statistics. In Figure 4(b), the normalized a_{rms} is plotted in presence of gravity for the same particle size range. There are several important observations. First, in contrast to the zero-gravity results, the rms acceleration initially increases with the particle size, especially in the horizontal direction. A peak value is reached at about $St \approx 1.2$. This can be explained qualitatively in terms of the preferential sweeping mechanism as identified in Wang and Maxey.[26] Due to the preferential sweeping, an inertial particle, when approaching a vortical structure, accelerates to the down flow side of the vortical structure, enhancing the acceleration changes in the horizontal direction (see Figure 5).

An important observation is that there is a clear difference in the rms acceleration values between the vertical and horizontal directions. While gravity enhances the rms acceleration in both directions, the effect is stronger in the direction perpendicular to the gravity. When $St \to 0$, one would expect that the normalized rms acceleration approaches one, but our results for the smallest St ($St = 0.06$) are still significantly less than one. There could be several reasons here: first, the empirical scaling of a_0 (Hill[24]) may not be accurate due to data fitting error, and second, the numerical results are subject to a significant statistical error when St is small (as in this case, a very small time step is needed and the computation becomes prohibitively expensive).

The experimental measurement of Volk *et al.*[2] for $St = 0.58$ at $R_\lambda = 850$ has a large uncertainty but falls consistently within our DNS data points. Further, accurate experimental data are required to precisely match the DNS data. Also, another data point of Volk *et al.*[2] for $St = 1.03$ at $R_\lambda = 180$ from their DNS is in agreement with our results within the standard deviations. We could not verify whether the acceleration results of Volk *et al.*[2] are averaged in all three dimensions or in one specific direction (vertical/horizontal).

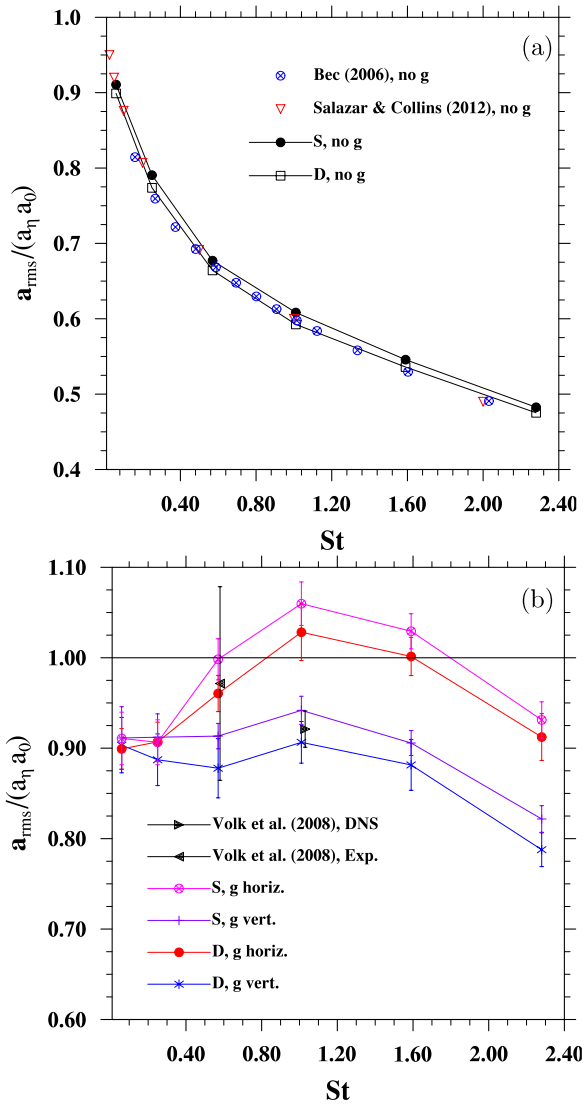

FIG. 4. The rms of particle acceleration for (a) non-sedimenting particles averaged over the three directions and (b) sedimenting particles. Legend: D denotes the deterministic forcing; S is for the stochastic forcing. The two single data points are from Volk *et al.*[2] for one experimental measurement ($St = 0.58$ at $R_\lambda = 850$), and one DNS data point ($St = 1.03$ at $R_\lambda = 180$).

In both horizontal and vertical directions, the stochastic forcing yields slightly larger values of rms acceleration (by up to 4.7%), for the similar reasons discussed above for non-sedimenting particles.

Now, we consider more results with the flow forced by the deterministic forcing only (with R_λ = 143 thereafter). For the rest of the paper, we limit the discussions to the use of deterministic forcing because (1) we found that there is no qualitative difference between the results from the two forcing schemes, (2) the effects of forcing for collision statistics have already been systematically discussed in our recent paper,[18] which showed that even the quantitative difference is small for small particles (say, less than 30 μm), and (3) the focus of the paper is on the comparison of results with gravity and results without gravity, and we do not want other topics to distract this focus. For two particle sizes (a = 50 and 60 μm or St = 1.59 and 2.28), the vertical and horizontal acceleration pdf are plotted in Figures 6 and 7, respectively. Two different levels of gravity are considered (**g** and 2**g**), along with the nonsedimenting case. The pdf is symmetric for the horizontal acceleration and as such only the pdf of positive horizontal acceleration is shown (Figure 7).

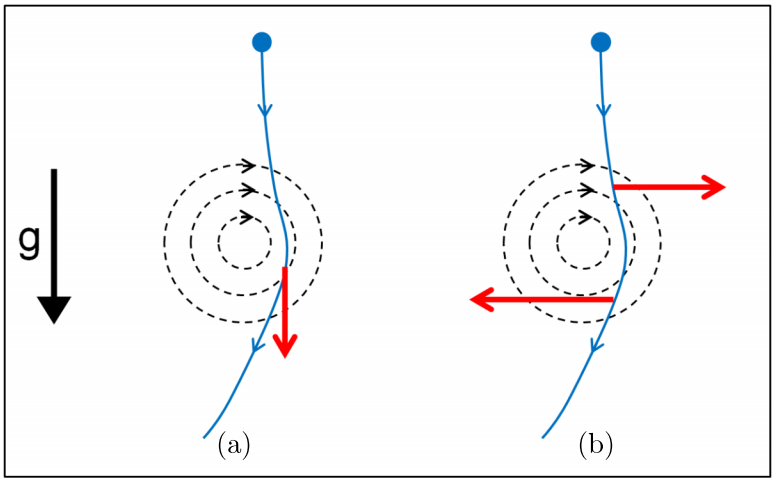

FIG. 5. Schematic of a sedimenting particle acceleration due to interaction with an eddy. Red arrows show the acceleration (a) in the vertical plane, (b) in the horizontal plane.

We observe that increasing the magnitude of gravitational acceleration broadens the tails of the particle acceleration pdf. This can be understood by the fact that increasing $|\mathbf{g}|$ will push the particles through intense fluid acceleration regions (vortex cores) which particles could avoid in absence of gravity. Since the turbulence is homogeneous and isotropic, the shorter particle-eddy interaction time leads to a narrower acceleration tails both in vertical and horizontal directions, as expected. A similar trend is observed for smaller Stokes numbers of $St = 0.57$ and 1.01. However, obtaining reliable pdf curves for smaller St become more difficult due to decreasing samples (implying smaller separation distances). The flatness (kurtosis) values of particle rms acceleration is provided in Table II.

To compare with experimental data, the particle acceleration is plotted in Figure 8, along with the results of Ayyalasomayajula *et al.*[1] and Volk *et al.*[2] We chose $St = 0.15$ and 0.58, respectively, from their experimental results because these Stokes numbers were the closest to our parameter setup. The turbulence parameters are completely different for these results. For example, the Reynolds numbers and dissipation rates of $R_\lambda = 850$ and $\epsilon = 25\ \mathrm{m^2/s^3}$ in Volk *et al.*[2] and $R_\lambda = 250$ and $\epsilon = 960\ \mathrm{cm^2/s^3}$ in Ayyalasomayajula *et al.*[1] are much larger than those of our DNS ($R_\lambda = 143$ and $\epsilon = 400\ \mathrm{cm^2/s^3}$). Therefore, the flow regimes are not similar and, with the available data to date, a rigorous comparison with experimental results is not feasible.

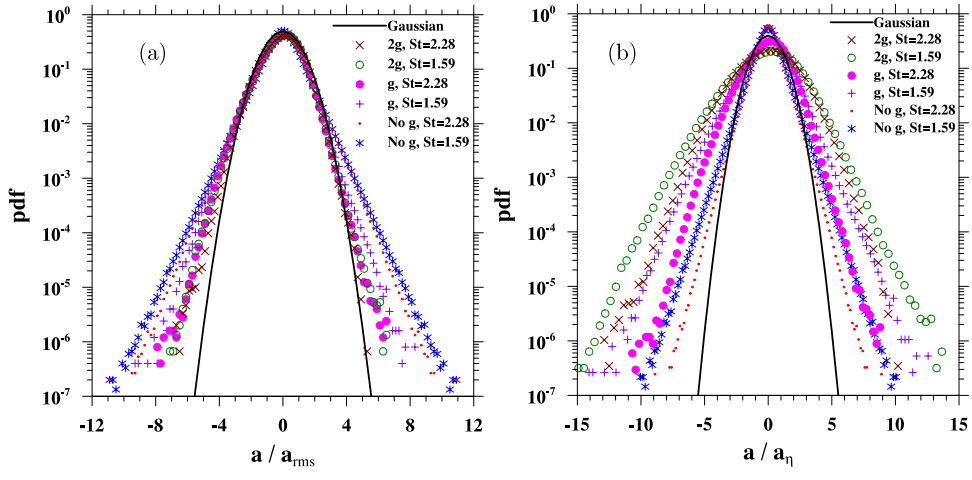

FIG. 6. (a) PDF of the vertical acceleration for 3 different values of gravitational acceleration. (b) the same data as (a) normalized by fluid acceleration at Kolmogorov scale.

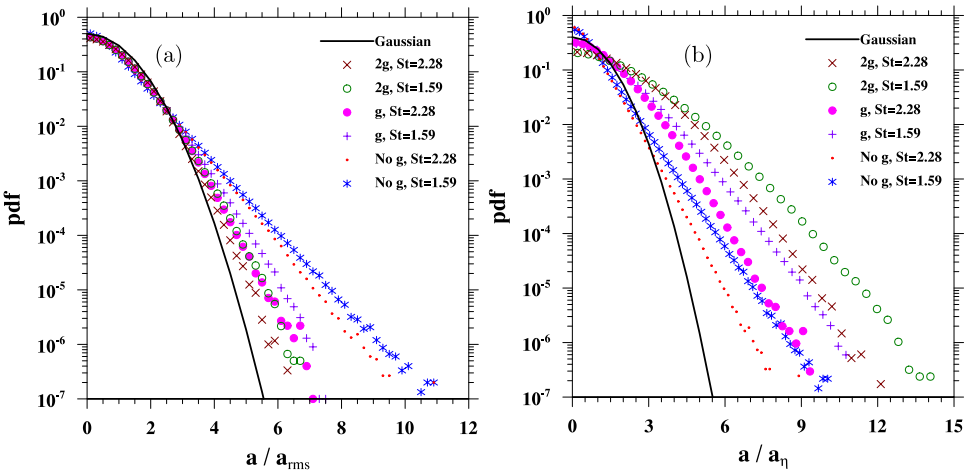

FIG. 7. (a) PDF of the horizontal acceleration for 3 different values of gravitational acceleration. Only the side of positive acceleration is shown as the PDF for horizontal acceleration is symmetric. (b) the same data as (a) normalized by fluid acceleration at Kolmogorov scale.

B. Radial relative velocity for monodisperse particle pairs

Next, we focus on the effect of particle acceleration on the radial relative velocity of nearly colliding particles. Over the past decades, different models have been introduced to compute the average RRV of particles in turbulence (e.g., Saffman and Turner,[27] Abrahamson,[28] Wang *et al.*,[29] Dodin and Elperin,[30] Zaichik *et al.*,[31] and Ayala *et al.*[32]), each of which makes a number of assumptions restricting their use to a limited parameter space (e.g., small particle inertia and no gravity). To provide a more complete understanding of how turbulence, particle inertia, and gravity contribute to the net radial relative velocity between two particles, following Grabowski and Wang,[14] we present an alternative analysis. Based on the particle equation of motion (Eq. (3)), the radial relative velocity can be decomposed into three parts: gravitational term (w_g), shear term (w_s), and differential acceleration term (w_a). Considering the Stokes drag, inertia and gravity, and assuming a small separation distance ($r = |\mathbf{r}| < \eta$), we take the dot product of the Eq. (3), written for $V^{(1)}$ and $V^{(2)}$, with $\mathbf{r}/|\mathbf{r}|$ yielding

$$w_r = \left[\mathbf{V}^{(1)}(t) - \mathbf{V}^{(2)}(t)\right] \cdot \frac{\mathbf{r}}{r} = w_g + w_s + w_a, \tag{5}$$

where

$$\begin{aligned} w_g &= \left[\tau_p^{(1)} - \tau_p^{(2)}\right] |\mathbf{g}| \cos(\alpha), \\ w_s &= \frac{r_i r_j}{r} s_{ij}, \\ w_a &= -\frac{r_j}{r}\left[\tau_p^{(1)} \frac{dV_j^{(1)}(t)}{dt} - \tau_p^{(2)} \frac{dV_j^{(2)}(t)}{dt}\right] \end{aligned} \tag{6}$$

TABLE II. Flatness of particle rms acceleration for the data on Figures 6 and 7.

	Figure 6			Figure 7		
St	No g	g	2g	No g	g	2g
1.59	5.34	4.11	3.56	5.34	4.01	3.59
2.28	4.92	3.58	3.23	4.92	3.55	3.25

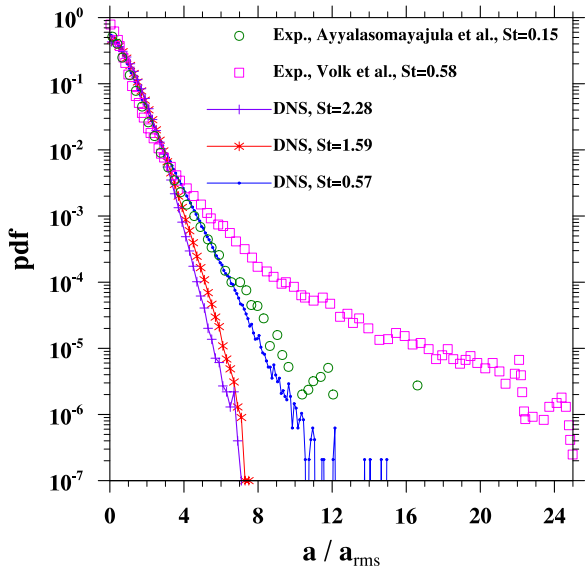

FIG. 8. PDF of the horizontal acceleration for sedimenting particles from DNS (at $R_\lambda = 143$ and $\epsilon = 400$ cm^2/s^3) in comparison with the experimental results of Ayyalasomayajula *et al.*[1] (at $R_\lambda = 250$ and $\epsilon = 960$ cm^2/s^3) and Volk *et al.*[2] (at $R_\lambda = 850$ and $\epsilon = 25$ m^2/s^3).

represent contributions from gravity, fluid shear, and particle differential acceleration, respectively (see Figure 9 for an illustration). Here, s_{ij} is the fluid strain rate and α is the angle between the relative velocity and the separation vector of the two particles. We proceed to study the properties and relative magnitude of each of the three mechanisms in the particle RRV which is the main focus for the remainder of this section.

In Figure 10, we plot the pdf of the normalized shear term $w_{s,11}$ for monodisperse particles (hence, denoted $w_{s,11}$ where subscript 11 refers to monodisperse cases) of $St = 0.57, 1.01$ and $St = 2.28$ in both sedimenting and non-sedimenting settings. The separation $|\mathbf{r}|$ is set to $2a$, the geometric collision radius. Note that the gravity term w_g is zero for monodisperse particles, although through coupling, gravity could still affect the other two terms. The close overlap of the curves for two Stokes numbers and two different levels of gravity shows that the shape of the probability distribution is not much affected by the gravity. Our simulations for other Stokes numbers ($St = 0.06, 0.25$, and 1.59 not plotted in Figure 10) further confirm that the effect of St on the pdf of the normalized $w_{s,11}$ is negligible for the aforementioned range of St. In the following plots, σ is the rms value of the plotted parameter. We note that the distribution of $w_{s,11}$ is negatively skewed indicating a bias of the relative motion of particle pairs at $|\mathbf{r}| = 2a$ toward a larger negative relative velocity. Table III summarizes the skewness of $w_{s,11}$ for the data on Figure 10. The skewed

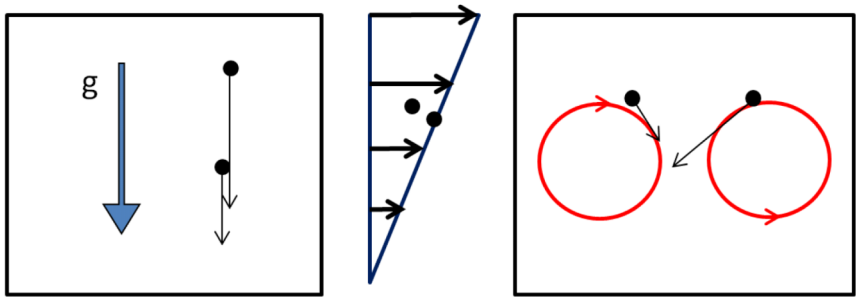

FIG. 9. From left to right w_g, w_s, and w_a represent contributions to relative velocity from gravity, fluid shear, and particle differential acceleration, respectively.

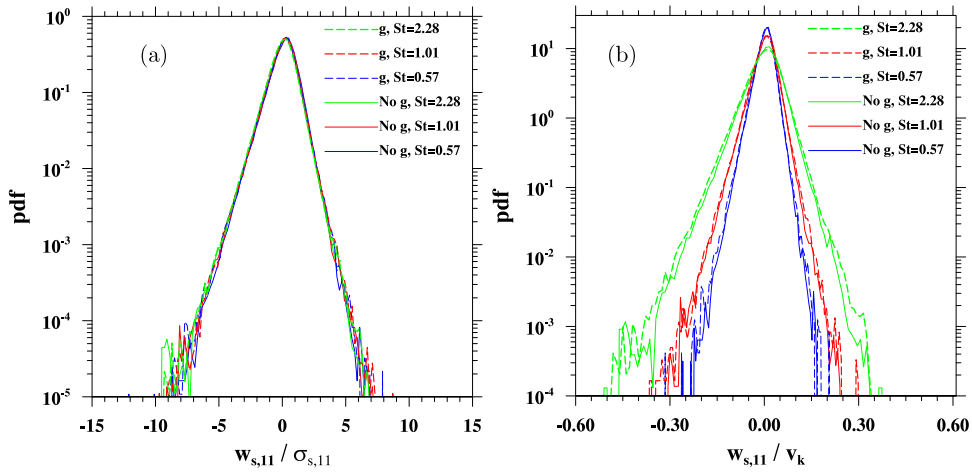

FIG. 10. (a) Pdf of the normalized relative velocity due to the shear term $w_{s,11}$. σ is the rms value of the plotted parameter. (b) the same data as (a) normalized by Kolmogorov velocity.

distribution of radial relative velocity at contact was first observed in Wang *et al.*[33] who also showed that the skewness is strongest when $St \sim 1$. We believe that this is caused by a biased sampling of inertial-particle pairs at $|\mathbf{r}| = 2a$. For non-sedimenting particles, a detailed investigation of the relative velocity was provided by Salazar and Collins.[34] Using relative velocity structure functions, they numerically studied the particle relative velocity statistics. In absence of gravity, they found that filtering is the dominant mechanism for pair relative velocity statistics at all St.

In Figure 11, we show the pdf of the relative motion due to the differential acceleration $w_{a,11}$ for monodisperse particles (namely, particle pairs of identical size). For the monodisperse case, w_a reduces to

$$w_{a,11} = -\tau_p^{(1)} \frac{r_j}{r} \left[\frac{dV_j^{(1)}(t)}{dt} - \frac{dV_j^{(2)}(t)}{dt} \right]. \tag{7}$$

The term in the square bracket is exactly the differential acceleration vector which after projection over separation vector yields the contribution of the relative acceleration to w_a. Only pairs with a separation distance close to the geometric collision radius ($2a - \delta < |\mathbf{r}| < 2a + \delta$) are considered with $\delta = 0.02a$.

The results in Figure 11(a) show that $w_{a,11}$ has a considerably broader tail than $w_{s,11}$ both in presence and in absence of gravity (i.e., compare panels of Figure 11 with those of Figure 10). Our results on Figure 11(b) along with Figure 10(b) show that the presence of gravity suppresses the tails of both pdf($w_{a,11}$) and pdf($w_{s,11}$) leading to a less intermittent behavior of $w_{a,11}$ and $w_{s,11}$. This is in agreement with the shorter residence time of a particle in a vortex when a particle moves in the presence of gravity. As a result, both particles in the pair experience weaker interactions with vortices yielding a less intermittent dynamics. Gravity has a considerable effect on narrowing the tails of pdf($w_{a,11}$) while the pdf($w_{s,11}$) is less affected. This finding is consistent with the results

TABLE III. Skewness (S) of $w_{s,11}$ and flatness (F) of $w_{a,11}$ for the data on Figures 10 and 11, respectively.

	S: Figure 10		F: Figure 11	
St	No g	g	No g	g
0.57	−0.11	−0.29	442.5	449.3
1.01	−0.26	−0.32	224.4	390.0
2.28	−0.44	−0.49	44.7	299.1

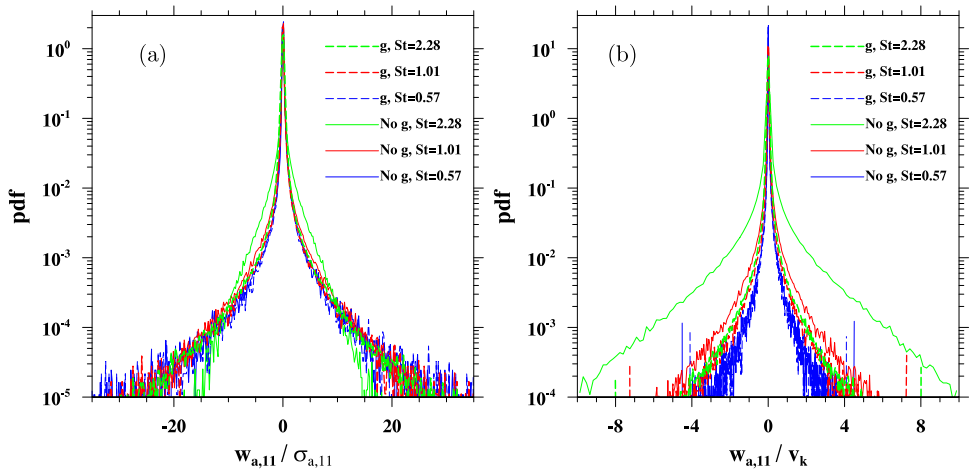

FIG. 11. (a) Pdf of the normalized relative velocity due to the relative acceleration term $w_{a,11}$. σ is the rms value of the plotted parameter. (b) the same data as (a) normalized by Kolmogorov velocity.

of Gustavsson *et al.*[35] where they found that gravity suppresses the tails of relative velocity above a certain critical Stokes number ($St^* \sim 0.4$). However, their results are obtained using a random two-dimensional flow field which may not realistically reproduce the dynamics of a three dimensional turbulence. We note that this wide tail of $w_{a,11}$ could lead, in some extreme cases, to a significant contribution of differential acceleration in widening the pdf tails of the radial relative velocity. We should emphasize that unlike $w_{s,11}$, pdf of $w_{a,11}$ is essentially symmetric. For the curves on Figure 11, the flatness (kurtosis) of $w_{a,11}$ is provided in Table III.

In Figure 12, the ratio of $\langle|w_s|\rangle/\langle|w_a|\rangle$ is plotted for monodisperse particles at $|\mathbf{r}| = 2a$. For both sedimenting and non-sedimenting pairs, the fluid shear is a dominant mechanism in radial relative velocity of small particles ($a < 30$ μm), while the differential acceleration becomes increasingly dominant for large particles ($a > 30$ μm). We observe that for large sedimenting particles,

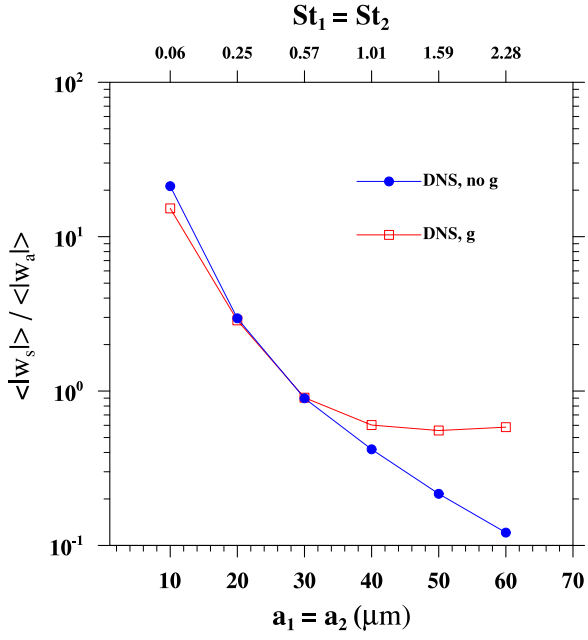

FIG. 12. The ratio $\langle|w_s|\rangle/\langle|w_a|\rangle$ for monodisperse cases as a function of particle radius, showing that the shear term is dominant for small particles, while the differential acceleration term becomes dominant for large particles.

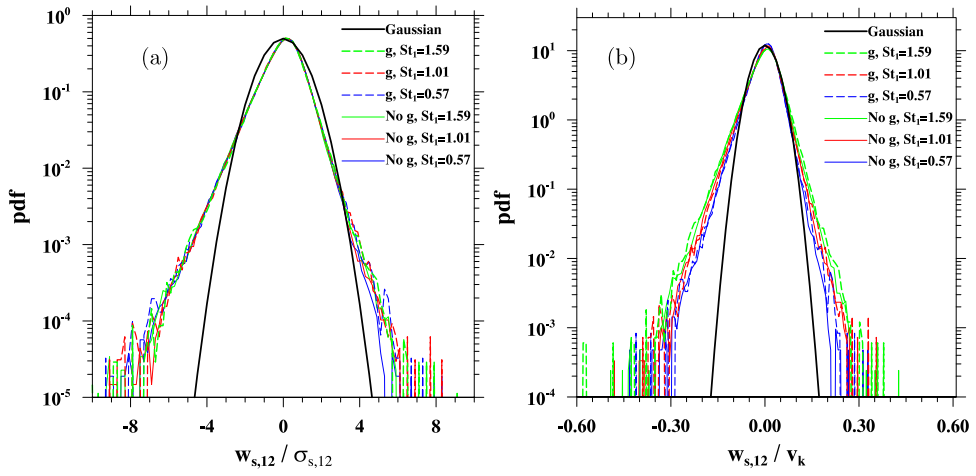

FIG. 13. (a) PDF of $w_{s,12}$ (bidisperse, $a_2 = 60\ \mu$m and $St_2 = 2.28$). (b) the same data as (a) normalized by Kolmogorov velocity.

$\langle|w_s|\rangle/\langle|w_a|\rangle$ approaches a plateau where w_s and w_a could both make substantial contributions to the radial relative velocity. For small particles, the ratio is essentially the same (with a maximum of 29% difference for 10 μm droplets) regardless of the presence of gravity. This may be interpreted as the negligible effect of gravity in terms of the following dimensionless parameter dictating the combined effect of sedimentation and particle inertia:

$$F_p = \frac{\tau_p^3 g^2}{v} = St \cdot Sv^2 \tag{8}$$

which represents the particle inertial response time to the residence time of a particle in an eddy (see Davila and Hunt[36] who first introduced this parameter). Interestingly, this parameter does not depend on the flow dissipation rate and is about one when the droplet radius is about 20 μm.[32] This implies that the gravity does not affect the relative acceleration of smaller monodisperse droplets due to turbulence. Only for larger droplets, the caustic effect appears which is consistent with the pdf curves shown in Figure 11.

C. Radial relative velocity for bidisperse particle pairs

In this section, we consider the radial relative motion between two particles of different radii a_1 and a_2. Again, we are interested in the radial relative velocity when the two particles are separated by the geometric contact distance ($R = a_1 + a_2$).

Figure 13 shows the pdf of the normalized shear contribution for bidisperse combinations (hence, denoted $w_{s,12}$ where subscript 12 refers to bidisperse cases) for $a_1 = 30, 40, 50\ \mu$m (or $St_1 = 0.57, 1.01, 1.59$) with a_2 fixed at 60 μm ($St_2 = 2.28$). The results of sedimenting particles are compared to those of non-sedimenting particles. Similar to the monodisperse case, the gravity has a negligible effect on the shape of the $pdf(w_s)$. Furthermore, the distribution of w_s is negatively skewed, similar to the monodisperse case. On the other hand, the gravity significantly affects the $pdf(w_a)$ for bidisperse particles (Figure 14). The $pdf(w_{a,12})$ approaches the Gaussian distribution and the intermittent tails have been significantly reduced in comparison with the mono-disperse results in Figure 11. In general, the pdfs for bidisperse particles have much narrow tails than those of monodisperse particles (e.g., compare Figure 14 with Figure 11). This implies that the acceleration term is less intermittent as the two particles in the pair become more dissimilar in size. This observation is consistent with the loss of correlation of concentration fluctuations[37] and rapid decrease of radial relative velocity for bidisperse particles (Ayala *et al.*[32] and Wang *et al.*[38]) when compared to monodisperse particles.

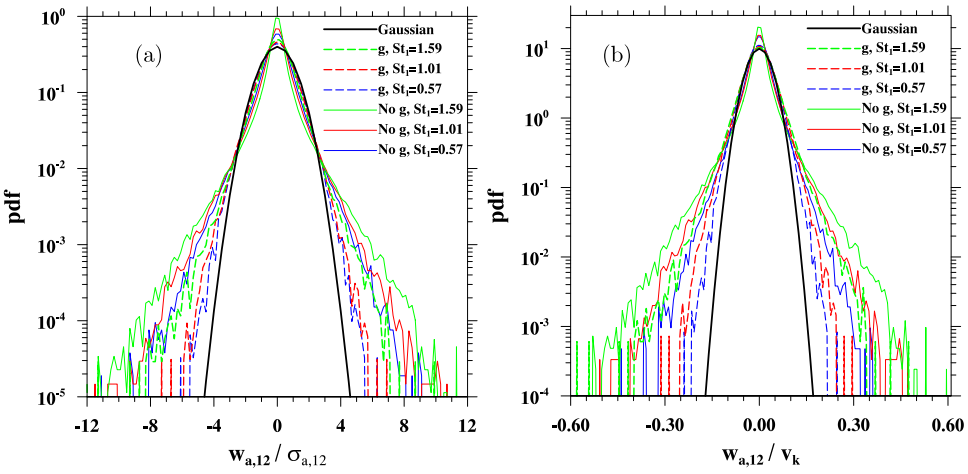

FIG. 14. (a) Pdf of $w_{a,12}$ (bidisperse, $a_2 = 60$ μm and $St_2 = 2.28$, $a_1 = 30$, 40, and 50 μm). (b) the same data as (a) normalized by Kolmogorov velocity.

For bidisperse pairs, Figure 13 shows that there is a negligible effect of gravity on $w_{s,12}$. Also the distribution of $w_{s,12}$ is negatively skewed indicating the bias of the colliding particles toward negative relative velocities. This behavior is similar to that of the monodisperse cases and due to the presence of particles in drifting regions of the fluid. The skewness values of $w_{s,12}$ is provided in Table IV. On the other hand, the effect of gravity on $w_{a,12}$ of bidisperse collisions (as plotted in Figure 14) is significant. For the curves on Figure 14, the flatness (kurtosis) of $w_{a,12}$ is provided in Table IV.

In Figure 15, we plot the ratio of the shear contribution (w_s) to that of the gravity term (w_g). In the context of cloud and rain droplets, the shear term appears to be negligible when compared to the gravity term, with the ratio being less than $<2\%$. In the same plot, we show the estimation of Grabowski and Wang[14] for $\langle|w_s|\rangle/\langle|w_g|\rangle$. We observe that their estimation of

$$\frac{\langle|w_s|\rangle}{\langle|w_g|\rangle} \approx \frac{\sqrt{\nu\epsilon}}{222.2g(a_1 - a_2)} \frac{1}{\cos(\alpha)} \tag{9}$$

predicts a valuable upper bound for the relative value of $\langle|w_s|\rangle/\langle|w_g|\rangle$. Average value of $\cos(\alpha) = 0.5$ is used to plot Eq. (9) in Figure 15.

In Figure 16, the ratio of the differential acceleration term (w_a) to the gravity term (w_g) is plotted. The differential acceleration term appears to be of the same order of magnitude, but smaller than the gravity term. The ratio is between 30% and 60%. Therefore, when gravity and differential acceleration are combined together, the actual enhancement factor relative to the gravity term is then expected to be $\sqrt{0.3^2 + 1^2} = 1.04$ to $\sqrt{0.6^2 + 1^2} = 1.17$, if the correlation between the gravity term and the acceleration term is neglected. Namely, turbulent acceleration can increase the radial relative velocity by 4%–17%, consistent with the results in previous studies Wang *et al.*,[39] Franklin

TABLE IV. Skewness (S) of $w_{s,12}$ and flatness (F) of $w_{a,12}$ for the data on Figures 13 and 14, respectively.

	S: Figure 13		F: Figure 14	
St_1	No g	g	No g	g
0.57	−0.65	−0.53	7.49	3.79
1.01	−0.61	−0.52	9.87	4.24
1.59	−0.62	−0.52	15.11	6.36

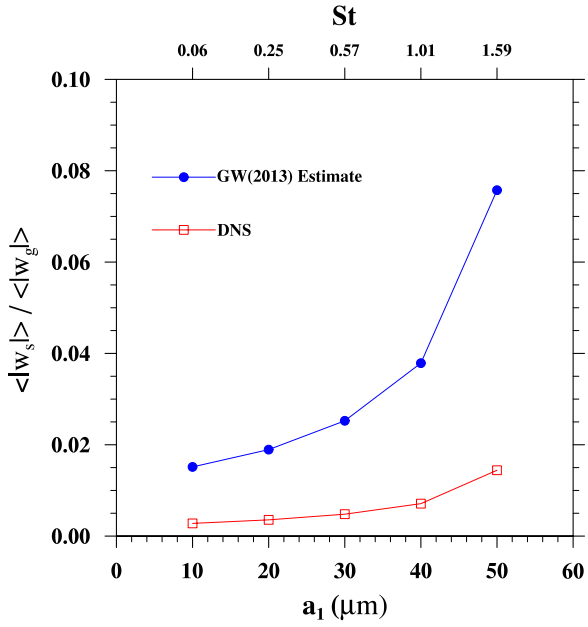

FIG. 15. The ratio of the shear contribution (w_s) to the gravity term (w_g) for bidisperse particles, with $a_2 = 60$ μm. DNS: current study, estimate: estimation of Grabowski and Wang.[14]

et al.,[40] and Ayala *et al.*[32] Grabowski and Wang[14] suggested a scaling analysis for this ratio,

$$\frac{\langle |w_a| \rangle}{\langle |w_g| \rangle} \approx \sqrt{\frac{11 + 7R_\lambda}{205 + R_\lambda}} \frac{\epsilon^{0.75}}{g\nu^{0.25}\cos(\alpha)}, \tag{10}$$

to estimate the relative importance of the particle differential acceleration. Using an average value of $\cos(\alpha) = 0.5$, Figure 16 shows that this estimate is reasonable.

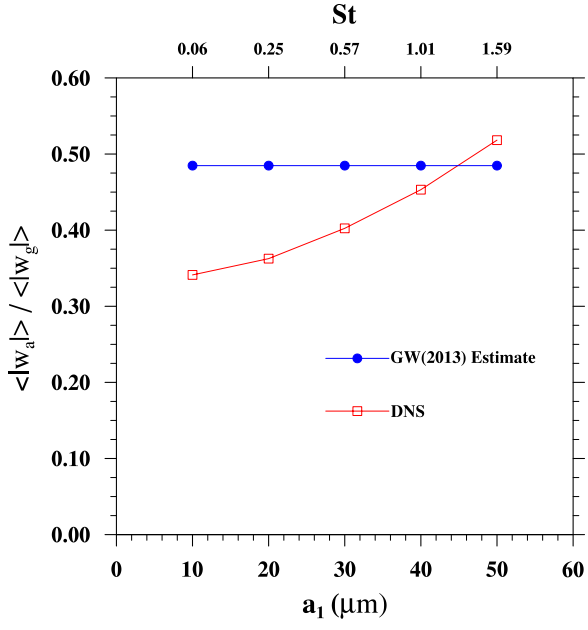

FIG. 16. The ratio of the differential acceleration term to the gravity term for bidisperse particles, with $a_2 = 60$ μm. DNS: current study, estimate: estimation of Grabowski and Wang.[14]

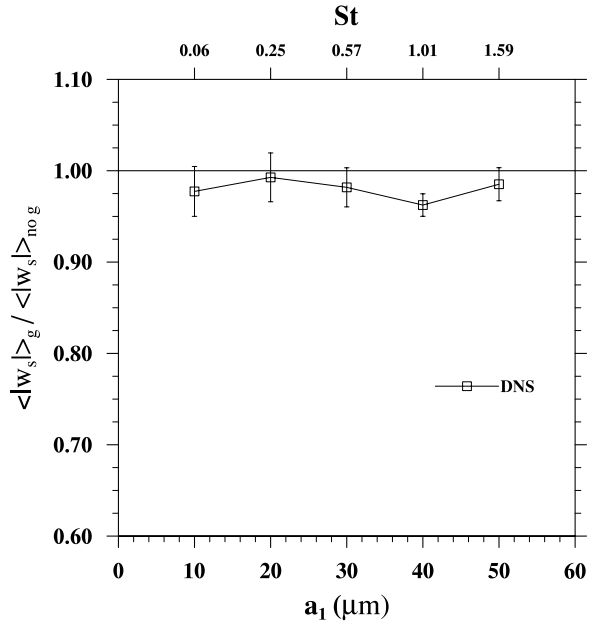

FIG. 17. The value of $\langle|w_s|\rangle$ with gravity relative to that without gravity, for bidisperse particles. $a_2 = 60\ \mu$m.

To obtain a quantitative understanding of the effect of gravity on w_s, we compare the values of w_s, with and without gravity, in Figure 17. We notice a small decrease ($<2\%$) in w_s when the gravity is present. Therefore, the magnitude of the shear term is almost independent of the gravity.

A similar plot is shown in Figure 18 for the differential acceleration term $\langle|w_a|\rangle$. In contrast to the shear term, the gravity enhances the acceleration term by roughly a factor of 2, but this enhancement is reduced when the particle sizes become similar. For sedimenting particles, the relative acceleration vector of the two particles is biased towards the vertical direction. For similar size particles, this relative acceleration is small because the response of two particles to local fluid flow becomes similar in magnitude and direction. Therefore, following Eq. (7), the terms inside the bracket (i.e., the relative acceleration) becomes smaller for similar size particles leading to smaller $\langle|w_a|\rangle_g$. However, for non-sedimenting particles, the fluid turbulence is the only accelerating mechanism causing a relative acceleration in all three directions (even for particles similar in size). Hence, the decrease in $\langle|w_a|\rangle_g$ is larger than that of $\langle|w_a|\rangle_{nog}$ leading to a decrease in the ratio of $\langle|w_a|\rangle_g/\langle|w_a|\rangle_{nog}$ when the particle sizes become similar.

Finally, to study the extent of coupling between the gravity term and the differential acceleration term, the cross correlation coefficient ρ_{ga} of w_g and w_a defined as

$$\rho_{ga} = \frac{\langle (w_g - \langle w_g\rangle)\,(w_a - \langle w_a\rangle)\rangle}{\sqrt{\langle (w_g - \langle w_g\rangle)^2\rangle}\sqrt{\langle (w_a - \langle w_a\rangle)^2\rangle}} \tag{11}$$

is shown in Figure 19 for bidisperse particles (for monodisperse cases, $w_g = 0$). A finite positive correlation coefficient of up to ~ 0.14 is observed between w_a and w_g. Furthermore, the coupling becomes increasingly stronger when the difference in particle sizes becomes smaller. The gravity likely reduces the particle-eddy interaction time, thus constantly interrupting the quasi-equilibrium between the inertial particle and the fluid turbulence. Consequently, the gravity led to larger particle accelerations in both horizontal and vertical directions compared to the no-gravity case, e.g., comparing Figures 4(b) and 4(a). This is the major reason for large relative acceleration observed in Figure 18. For bidisperse pairs, the positive correlation coefficient shown in Figure 19 implies that, when the pair is oriented vertically due to gravity, the differential acceleration is also larger. The latter could be another reason to expect a large differential acceleration when compared to the no-gravity case.

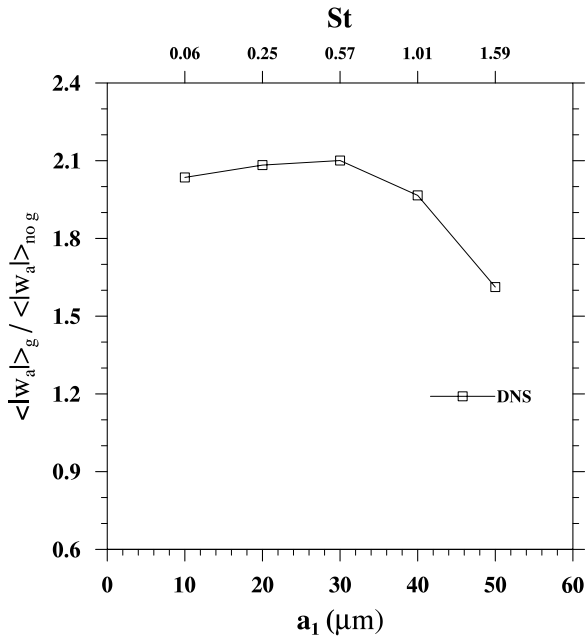

FIG. 18. The ratio of $\langle|w_a|\rangle$ with gravity to that without gravity. $a_2 = 60\ \mu$m.

IV. ASYMPTOTIC ANALYSIS OF EFFECT OF GRAVITY ON PARTICLE ACCELERATION VARIANCE

In Figure 4(b), the normalized a_{rms} is shown in the presence of gravity. The results in this figure can be explained using the theory presented in the following. We develop two analytical approaches to the problem, each of which may be used for different cases of gravity and droplet inertia. Note that in the following derivations, d/dt is the total derivative in particle reference frame

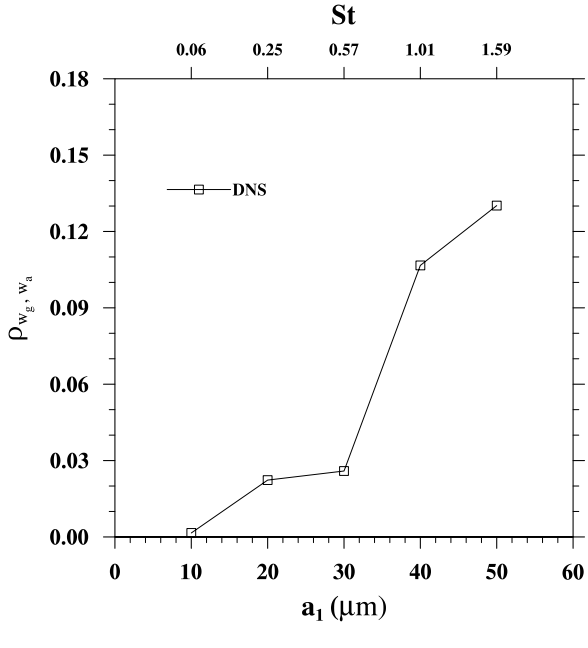

FIG. 19. The correlation coefficient between the gravity term and the differential acceleration term. $a_2 = 60\ \mu$m.

and is defined as $\frac{d}{dt} = \frac{\partial}{\partial t} + \mathbf{V}\cdot\nabla$, while D/Dt is the total derivative in fluid reference frame and is defined as $\frac{D}{Dt} = \frac{\partial}{\partial t} + \mathbf{U}\cdot\nabla$.

A. The first approach: Gravity without inertia

We shall first develop an approximate expression of particle acceleration under the limit of $St \to 0$ and finite Sv, where Sv is the terminal velocity of the particle normalized by Kolmogorov velocity. In the context of cloud droplets, we can show that $St \sim \epsilon^{0.5}$ and $Sv \sim 1/\epsilon^{0.25}$. Therefore, the limiting case corresponds to $St \to 0$ (or alternatively, a very large gravitational acceleration). Under this limit, the droplet inertia can be neglected but the sedimentation must be retained. Let the terminal velocity be denoted by $\mathbf{W} = (0,0,-w)$ with the gravity pointing in the negative x_3 direction. In this limit, the particle velocity can be written in an exact form as a superposition of local fluid velocity and terminal velocity (if we assume the particle has reached its terminal velocity), $\mathbf{V} = \mathbf{U} + \mathbf{W}$. By taking the d/dt derivative, the particle acceleration is $\frac{d\mathbf{V}}{dt} = \frac{d\mathbf{U}}{dt} = \frac{\partial \mathbf{U}}{\partial t} + \mathbf{V}\cdot\nabla\mathbf{U}$ and substituting $\mathbf{V} = \mathbf{U} + \mathbf{W}$ leads to $\frac{d\mathbf{V}}{dt} = \left(\frac{\partial \mathbf{U}}{\partial t} + \mathbf{U}\cdot\nabla\mathbf{U}\right) + \mathbf{W}\cdot\nabla\mathbf{U}$. Substituting the definition of fluid acceleration $D\mathbf{U}/Dt$ yields

$$\frac{d\mathbf{V}}{dt} = \frac{D\mathbf{U}}{Dt} + (\mathbf{W}\cdot\nabla)\,\mathbf{U}. \tag{12}$$

$\mathbf{U} = (u_1, u_2, u_3)$ and $\mathbf{V} = (v_1, v_2, v_3)$ are denoted as the instantaneous fluid and particle velocities, respectively, both measured at particle center. Now, substituting $\mathbf{W} = (0,0,-w)$, we handle the horizontal and vertical components of (12) separately.

1. The horizontal component becomes $\frac{dv_1}{dt} \approx \frac{Du_1}{Dt} - w\frac{\partial u_1}{\partial x_3}$. Denoting $\frac{dv_1}{dt} = a_{p1}$ and $\frac{Du_1}{Dt} = a_{f1}$, the average particle acceleration variance in the horizontal direction is

$$\langle a_{p1}^2\rangle \approx \langle a_{f1}^2\rangle + w^2\left\langle\left(\frac{\partial u_1}{\partial x_3}\right)^2\right\rangle - 2w\left\langle a_{f1}\frac{\partial u_1}{\partial x_3}\right\rangle. \tag{13}$$

   Assuming a homogeneous isotropic turbulence and reducing the 2nd term yields

$$\langle a_{p1}^2\rangle \approx \langle a_{f1}^2\rangle + w^2\left(\frac{2\epsilon}{15\nu}\right) - 2w\left\langle a_{f1}\frac{\partial u_1}{\partial x_3}\right\rangle. \tag{14}$$

   Retaining the $O(w^2)$ term on the RHS (since $Sv >> 1$), the particle acceleration in horizontal direction reduces to

$$\langle a_{p1}^2\rangle \approx \langle a_{f1}^2\rangle + w^2\left(\frac{2\epsilon}{15\nu}\right). \tag{15}$$

2. The vertical component becomes $\frac{dv_3}{dt} \approx \frac{Du_3}{Dt} - w\frac{\partial u_3}{\partial x_3}$. Denoting $\frac{dv_3}{dt} = a_{p3}$ and $\frac{Du_3}{Dt} = a_{f3}$, the average particle acceleration variance in the vertical direction is obtained as

$$\langle a_{p3}^2\rangle \approx \langle a_{f3}^2\rangle + w^2\left\langle\left(\frac{\partial u_3}{\partial x_3}\right)^2\right\rangle - 2w\left\langle a_{f3}\frac{\partial u_3}{\partial x_3}\right\rangle, \tag{16}$$

   which by using the homogeneous isotropic turbulence assumption to reduce the 2nd term yields

$$\langle a_{p3}^2\rangle \approx \langle a_{f3}^2\rangle + w^2\left(\frac{\epsilon}{15\nu}\right) - 2w\left\langle a_{f3}\frac{\partial u_3}{\partial x_3}\right\rangle. \tag{17}$$

   Now, retaining the $O(w^2)$ term on the RHS (since $Sv >> 1$), the particle acceleration in the vertical direction reduces to

$$\langle a_{p3}^2\rangle \approx \langle a_{f3}^2\rangle + w^2\left(\frac{\epsilon}{15\nu}\right). \tag{18}$$

B. The first approach: Inertial particles without gravity

The small-St asymptotic limit without gravity was first introduced in Maxey,[41] which was later widely used in many publications. According to DNS data, this asymptotic limit typically holds true for $St < 0.05$ (Chun *et al.*[42]) or $St < 0.1$ (Ferry *et al.*[43]) depending on the type of statistics that is being examined. We start from the equation of motion for a small rigid particle considering the Stokes drag, namely, $\frac{d\mathbf{V}}{dt} = -\frac{\mathbf{V}-\mathbf{U}}{\tau_p}$. Therefore, the particle velocity is $\mathbf{V} = \mathbf{U} - \tau_p \frac{d\mathbf{V}}{dt}$. Now, approximating $d\mathbf{V}/dt$ with $D\mathbf{U}/Dt$, to the order τ_p, we will have $\mathbf{V} \approx \mathbf{U} - \tau_p \frac{D\mathbf{U}}{Dt}$. Taking the $\frac{d}{dt}$ derivative to obtain particle acceleration yields

$$\frac{d\mathbf{V}}{dt} \approx \frac{d\mathbf{U}}{dt} - \tau_p \frac{d}{dt}\left(\frac{D\mathbf{U}}{Dt}\right) \tag{19}$$

which is equal to

$$\frac{d\mathbf{V}}{dt} \approx \frac{D\mathbf{U}}{Dt} + (\mathbf{V}-\mathbf{U})\cdot\nabla\mathbf{U} - \tau_p \frac{d}{dt}\left(\frac{D\mathbf{U}}{Dt}\right), \tag{20}$$

leading to

$$\frac{d\mathbf{V}}{dt} \approx \frac{D\mathbf{U}}{Dt} - \tau_p \frac{D\mathbf{U}}{Dt}\cdot\nabla\mathbf{U} - \tau_p \frac{d}{dt}\left(\frac{D\mathbf{U}}{Dt}\right). \tag{21}$$

Now, approximating the d/dt derivative in the last term with D/Dt to the order τ_p yields

$$\mathbf{a}_p \approx \mathbf{a}_f - \tau_p \left(\mathbf{a}_f \cdot \nabla\mathbf{U} + \frac{D\mathbf{a}_f}{Dt}\right). \tag{22}$$

Since there is no gravity and the acceleration is considered spatially isotropic, we take one component of the acceleration as $a_{p1} \approx a_{f1} - \tau_p \left(\mathbf{a}_f \cdot \nabla u_1 + \frac{Da_{f1}}{Dt}\right)$ and compute the acceleration variance accordingly,

$$\begin{aligned}\langle a_{p1}^2\rangle \approx \langle a_{f1}^2\rangle &+ {\tau_p}^2\left\langle\left(\mathbf{a}_f\cdot\nabla u_1\right)^2\right\rangle + {\tau_p}^2\left\langle\left(\frac{Da_{f1}}{Dt}\right)^2\right\rangle \\ &- 2\tau_p\langle a_{f1}\mathbf{a}_f\cdot\nabla u_1\rangle - 2\tau_p\left\langle a_{f1}\frac{Da_{f1}}{Dt}\right\rangle \\ &+ {\tau_p}^2\left\langle\mathbf{a}_f\cdot\nabla u_1\frac{Da_{f1}}{Dt}\right\rangle.\end{aligned} \tag{23}$$

Using the proper scales of the flow to estimate the terms on the RHS and introducing the b_j coefficients, we have

$$\langle a_{p1}^2\rangle \approx \langle a_{f1}^2\rangle\left\{1 + b_1{\tau_p}^2\left(\frac{u'}{\lambda}\right)^2 + b_2\frac{\tau_p^2}{\tau_k^2} + b_3\tau_p\frac{u'}{\lambda} + b_4\frac{\tau_p}{\tau_k} + b_5{\tau_p}^2\frac{u'}{\lambda\tau_k}\right\}, \tag{24}$$

which after assuming a homogeneous isotropic turbulence, we obtain an asymptotic form as

$$\langle a_{p1}^2\rangle \approx \langle a_{f1}^2\rangle\left\{1 - c_1 St - c_2 St^2\right\}. \tag{25}$$

C. The first approach: Combining gravity and particle inertia

Finally, if we assume a small particle ($St << 1$), the total effects of gravity and inertia on the difference between particle and fluid acceleration variance (i.e., $\langle a_{pi}^2\rangle - \langle a_{fi}^2\rangle$) may be superposed to yield

$$\langle a_{pi}^2\rangle \approx \langle a_{fi}^2\rangle\left\{1 - c_1 St - c_2 St^2\right\} + A_i w^2\left(\frac{\epsilon}{15\nu}\right), \tag{26}$$

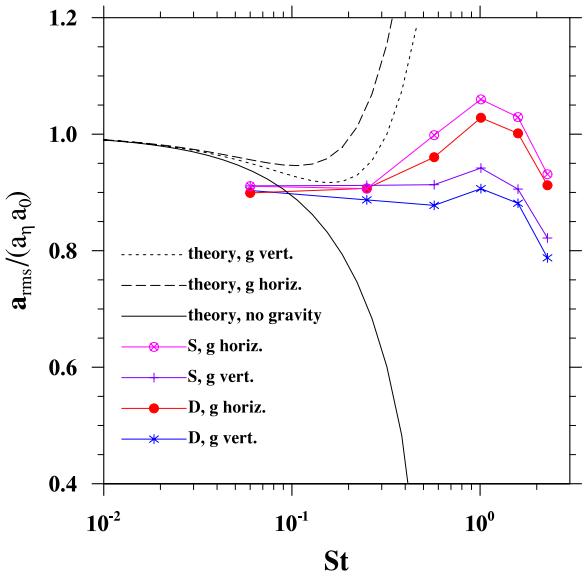

FIG. 20. Theoretical prediction for particle rms acceleration in comparison with DNS. Legend: D denotes the deterministic forcing; S is for the stochastic forcing.

where $A_i = 1$ for gravity direction, otherwise $A_i = 2$. This expression may be further simplified by assuming $\langle a_{fi}^2 \rangle \approx c_3 (v_k/\tau_k)^2$ which leads to

$$\frac{\langle a_{pi}^2 \rangle}{\langle a_{fi}^2 \rangle} \approx 1 - c_1 St - c_2 St^2 + c_3 \frac{A_i}{15} Sv^2. \tag{27}$$

From this analysis, it is clear that gravity correlates with particle acceleration variance both in the horizontal and the vertical directions. This results in an increase in particle acceleration variance in both directions. Furthermore, the effect of gravity on the horizontal acceleration variance is approximately twice stronger than that in the gravity direction. Back to Figure 4(b), this explains the reason why rms values of acceleration are larger in horizontal direction.

D. The second approach: Gravity and inertia together

This is an alternative and a more consistent approach. If gravity and inertia are considered simultaneously, we use the asymptotic expression of Balachandar and Eaton,[44]

$$\frac{d\mathbf{V}}{dt} \approx \frac{D\mathbf{U}}{Dt} - \tau_p \frac{D\mathbf{U}}{Dt} + \tau_p w \frac{\partial \mathbf{U}}{\partial x_3}, \tag{28}$$

which leads to the following expression for particle acceleration:

$$a_{pi} \approx a_{fi} - \tau_p \frac{Da_{fi}}{Dt} - w \frac{\partial u_i}{\partial x_3} + \tau_p \left(w \frac{\partial u_j}{\partial x_3} - \frac{Du_j}{Dt} \right) \frac{\partial u_i}{\partial x_j} + \tau_p \left(w \frac{Du_i}{Dt} \right) + O(\tau_p^2). \tag{29}$$

Now, the horizontal component of the acceleration variance becomes

$$\langle a_{p1}^2 \rangle \approx \langle a_{f1}^2 \rangle \left\{ 1 - 2St + 2\sqrt{2} c St \frac{w}{v_k} \frac{R_\lambda^{0.5}}{15^{0.75} a_0} + \frac{2}{15 a_0^2} \left(\frac{w}{v_k} \right)^2 \right\}, \tag{30}$$

and the vertical component of the acceleration variance is

$$\langle a_{p3}^2 \rangle \approx \langle a_{f3}^2 \rangle \left\{ 1 - 2St + 2c St \frac{w}{v_k} \frac{R_\lambda^{0.5}}{15^{0.75} a_0} + 2\tau_p w \left\langle u_j \frac{\partial a_{f3}}{\partial x_j} \frac{\partial u_3}{\partial x_3} \right\rangle + \frac{1}{15 a_0^2} \left(\frac{w}{v_k} \right)^2 \right\}. \tag{31}$$

Considering the dominance of gravity in this study (i.e., $Sv >> 1$), the last term of (31) is of order w^2 and is retained. However, among the two terms of $O(w)$ (the third and the fourth term), we retain the third term because it carries the c coefficient allowing us to fit this theory to DNS data to the extent possible. Therefore, the cross correlation term in (31) can safely be neglected. Consequently, for any positive c, the RHS of (30) will be larger than the RHS of (31) thus yielding a higher rms acceleration for particles in the horizontal direction. Further, (30) and (31) imply that when the gravitational settling dominates (large Sv), the particle acceleration variance might exceed that of a fluid element. To compare with our DNS results, in Figure 20, we have plotted the normalized a_{rms} using equations (30) and (31). Our results show that the parameter c should approximately be in the range of $0.03 - 0.1$ to qualitatively match the DNS results. (In this figure, we use $c = 0.04$.) The exact matching between the DNS results and the theory is not achieved mainly because the theory is accurate only for small St while the DNS results are obtained for droplets with finite St. This discrepancy between the theory and DNS data at smallest St number could be due to numerical integration errors and the neglect of cross correlation terms in the theory.

V. SUMMARY AND CONCLUSIONS

We have studied the effects of gravity on inertial particle acceleration and its effect on the contribution of differential acceleration to the radial relative velocity of inertial particles in a homogeneous isotropic turbulence. A newly developed massively parallel MPI code was employed to simulate the flow and dynamics of the droplets at flow Reynolds numbers up to $R_\lambda = 143$, using a 256^3 grid resolution with $O(10^6)$ droplets. For validation purposes, we reproduced the acceleration statistics of Bec *et al.*[7] and Salazar and Collins[8] using both stochastic and deterministic forcing schemes for non-sedimenting particles (i.e., with the gravitational acceleration set to zero).

We have shown that the gravity plays an important role in particle acceleration statistics. Specifically, we found that

1. A peak value of particle acceleration variance appears in both the horizontal and the vertical directions at about $St \sim 1.2$, at which both the particle horizontal and vertical accelerations clearly exceed the fluid-element acceleration. We note that as shown in Figure 5, the gravity pushes the particles to pass through turbulent eddy cores as such constantly interrupting quasi-equilibrium of a droplet's response to local turbulent motion. In other words, with gravity droplets would be less likely to reach quasi-equilibrium with the local turbulent motion, thus enhancing the droplet acceleration variance.
2. At the same time, we found that gravity amplifies extreme acceleration events both in the vertical and horizontal directions via the same mechanism, and thus effectively reduces the inertial filtering mechanism.

We developed a theory to explain the effects of gravity and turbulence on the horizontal and vertical acceleration variance of inertial particles. For a small particle ($St << 1$), the total effects of gravity and inertia on particle acceleration variance in the horizontal and vertical directions are approximated by (30) and (31). The particle rms acceleration in the horizontal direction is found to be higher than that in the vertical direction. We discussed that when the gravitational settling dominates (large Sv) the particle acceleration variance could even exceed that of a fluid element. We found that the fitting parameter c is in the range of $0.03 - 0.1$ and demonstrated that using $c = 0.04$, the theory qualitatively agrees with our DNS results for small droplet Stokes numbers in the sense that both yield a larger horizontal particle acceleration variance when compared to the vertical particle acceleration variance.

By decomposing the radial relative velocity of particles into three parts: the gravitational term (w_g), the shear term (w_s), and the differential acceleration term (w_a), we were able to study the effects of gravity on each of the three terms when the particles are at contact. For monodisperse particles, our results show that the presence of gravity does not have a significant effect on the shear term w_s. On the other hand, gravity suppresses the tails of $pdf(w_a)$. This could result from the lower particle-eddy interaction time in presence of gravity. Our results show that the $pdf(w_s)$ is negatively skewed while the $pdf(w_a)$ remains sufficiently symmetric.

For bidisperse particles, we found that gravity can decrease the average $|w_s|$ by pushing the particles into vortices where the local fluid shear is smaller. This decrease, however, is negligible (~2%). Therefore $|w_s|$ could be considered unaffected by gravity. We found that for bidisperse particles, the $pdf(w_s)$ is asymmetric while $pdf(w_a)$ is symmetric.

We also found that the differential acceleration term is positively correlated with the gravity term, and this correlation is stronger when the difference in particle radii becomes smaller. We demonstrated that the pdf tails of w_a is wider than the pdf tails of w_s, implying that the intermittent behavior of fluid acceleration is transferred to particle radial relative velocity mainly through the differential acceleration mechanism.

We emphasize that the focus of this paper is on particle acceleration and relative velocity for monodisperse particles, which we believe have not been discussed systematically in the literature. We set forward the preliminary discussions on the RRV for bidisperse distributions in Sec. III C. A more complete discussion of RRV for bidisperse and polydisperse distributions is the subject of future publications. Since particles are assumed to be non-interacting point particles, in principle, the statistics of a polydisperse size distribution can be evaluated by summing over groups of monodisperse and bidisperse particle pairs. A full discussion of the pdf of various contributions to the relative velocity, for different St and Sv as well as separation distances larger than the geometric collision radius, could be a topic for future research. We believe that this study not only extends the knowledge on acceleration statistics of sedimenting inertial particles but it also provides insights to better parameterize the radial relative velocity of inertial particles in turbulence. Additional simulations and analysis are needed to fully understand the effects of R_λ, flow dissipation rate, and particle-particle hydrodynamic interactions on the radial relative velocity.

ACKNOWLEDGMENTS

This work is supported by the National Science Foundation (NSF) under Grant Nos. AGS-1139743, ATM-0527140, ATM-0730766, OCI-0904534, and CRI-0958512. Computing resources are provided by National Center for Atmospheric Research (NCAR UDEL0001, CISL-35751014, and CISL-35751015). A generous computational support from XSEDE project ATM130019 (on Stampede platform) is highly acknowledged. The authors would like to express sincere gratitude to Interdisciplinary Centre for Mathematical and Computational Modelling (ICM) at Warsaw University for providing computational resources (Grant No. G49-15).

[1] S. Ayyalasomayajula, A. Gylfason, L. R. Collins, E. Bodenschatz, and Z. Warhaft, "Lagrangian measurements of inertial particle accelerations in grid generated wind tunnel turbulence," Phys. Rev. Lett. **97**, 144507 (2006).
[2] R. Volk, E. Calzavarini, G. Verhille, D. Lohse, N. Mordant, J.-F. Pinton, and F. Toschi, "Acceleration of heavy and light particles in turbulence: Comparison between experiments and direct numerical simulations," Physica D **237**, 2084 (2008).
[3] N. M. Qureshi, U. Arrieta, C. Baudet, A. Cartellier, Y. Gagne, and M. Bourgoin, "Acceleration statistics of inertial particles in turbulent flow," Eur. Phys. J. B **66**, 531 (2008).
[4] E. Calzavarini, R. Volk, M. Bourgoin, E. Leveque, J.-F. Pinton, and F. Toschi, "Acceleration statistics of finite-sized particles in turbulent flow: The role of Faxen forces," J. Fluid Mech. **630**, 179 (2009).
[5] R. Volk, E. Calzavarini, E. Leveque, and J.-F. Pinton, "Dynamics of inertial particles in a turbulent von Karman flow," J. Fluid Mech. **668**, 223 (2011).
[6] V. N. Prakash, Y. Tagawa, E. Calzavarini, J. M. Mercado, F. Toschi, D. Lohse, and C. Sun, "How gravity and size affect the acceleration statistics of bubbles in turbulence," New J. Phys. **14**, 105017 (2012).
[7] J. Bec, L. Biferale, G. Boffetta, A. Celani, M. Cencini, A. S. Lanotte, S. Musacchio, and F. Toschi, "Acceleration statistics of heavy particles in turbulence," J. Fluid Mech. **550**, 349 (2006).
[8] J. P. L. Salazar and L. R. Collins, "Inertial particle acceleration statistics in turbulence: Effects of filtering, biased sampling and flow topology," Phys. Fluids **24**, 083302 (2012).
[9] V. Lavezzo, A. Soldati, S. Gerashchenko, Z. Warhaft, and L. R. Collins, "On the role of gravity and shear on the acceleration of inertial particles in near-wall turbulence," J. Fluid Mech. **658**, 229 (2010).
[10] S. Gerashchenko, N. S. Sharp, S. Neuscamman, and Z. Warhaft, "Lagrangian measurements of inertial particle accelerations in a turbulent boundary layer," J. Fluid Mech. **617**, 255 (2008).
[11] R. Onishi, K. Takahashi, and S. Komori, "Influence of gravity on collisions of monodispersed droplets in homogeneous isotropic turbulence," Phys. Fluids **21**, 125108 (2009).
[12] Y. N. Park and C. H. Lee, "Gravity-driven clustering of inertial particles in turbulence," Phys. Rev. E **89**, 061004(R) (2014).
[13] I. M. Mazzitelli and D. Lohse, "Lagrangian statistics for fluid particles and bubbles in turbulence," New J. Phys. **6**, 203 (2004).
[14] W. W. Grabowski and L.-P. Wang, "Growth of cloud droplets in a turbulent environment," Annu. Rev. Fluid Mech. **45**, 293 (2013).

[15] N. P. Sullivan, S. Mahalingam, and R. M. Kerr, "Deterministic forcing of homogeneous isotropic turbulence," Phys. Fluids **6**, 1612 (1994).
[16] V. Eswaran and S. B. Pope, "An examination of forcing in direct numerical simulations of turbulence," Comput. Fluids **16**, 257 (1988).
[17] P. K. Yeung, J. G. Brasseur, and Q. Z. Wang, "Dynamics of direct large-small scale couplings in coherently forced turbulence: Concurrent physical- and Fourier-space views," J. Fluid Mech. **283**, 43-95 (1995).
[18] B. Rosa, H. Parishani, O. Ayala, W. W. Grabowski, and L.-P. Wang, "Kinematic and dynamic collision statistics of cloud droplets from high resolution simulations," New J. Phys. **15**, 045032 (2013).
[19] B. Rosa, H. Parishani, O. Ayala, and L.-P. Wang, "Effects of forcing time scale on the simulated turbulent flows and turbulent collision statistics of inertial particles," Phys. Fluids **27**, 015105 (2015).
[20] O. Ayala and L.-P. Wang, "Parallel implementation and scalability analysis of 3D fast Fourier transform using 2D domain decomposition," Parallel Comput. **39**, 58-77 (2013).
[21] O. Ayala, H. Parishani, L. Chen, B. Rosa, and L.-P. Wang, "DNS of hydrodynamically interacting droplets in turbulent clouds: Parallel implementation and scalability analysis using 2D domain decomposition," Comput. Phys. Commun. **185**, 3269-3290 (2014).
[22] C. E. Torres, H. Parishani, O. Ayala, L. F. Rossi, and L.-P. Wang, "Analysis and parallel implementation of a forced N-body problem," J. Comput. Phys. **245**, 235-258 (2013).
[23] P. Moin and K. Mahesh, "Direct numerical simulation: A tool in turbulence research," Annu. Rev. Fluid Mech. **30**, 539-578 (1998).
[24] R. J. Hill, "Scaling of acceleration in locally isotropic turbulence," J. Fluid Mech. **452**, 361-370 (2002).
[25] B. L. Sawford, P. K. Yeung, M. S. Borgas, P. Vedula, A. La Porta, A. M. Crawford, and E. Bodenschatz, "Conditional and unconditional acceleration statistics in turbulence," Phys. Fluids **15**, 3478 (2003).
[26] L.-P. Wang and M. R. Maxey, "Settling velocity and concentration distribution of heavy particles in a forced isotropic and homogeneous turbulence," J. Fluid Mech. **256**, 27 (1993).
[27] P. G. Saffman and J. S. Turner, "On the collision of drops in turbulent clouds," J. Fluid Mech. **1**, 16 (1956).
[28] J. Abrahamson, "Collision rates of small particles in a vigorously turbulent fluid," Chem. Eng. Sci. **30**, 1371 (1975).
[29] L.-P. Wang, A. Wexler, and Y. Zhou, "Statistical mechanical descriptions of turbulent coagulation," Phys. Fluids **10**, 2647 (1998).
[30] Z. Dodin and T. Elperin, "On the collision rate of particles in turbulent flow with gravity," Phys. Fluids **14**, 2921 (2002).
[31] L. I. Zaichik, O. Simonin, and V. M. Alipchenkov, "Two statistical models for predicting collision rates of inertial particles in homogeneous isotropic turbulence," Phys. Fluids **15**, 2995 (2003).
[32] O. Ayala, B. Rosa, L.-P. Wang, and W. W. Grabowski, "Effects of turbulence on the geometric collision rate of sedimenting droplets: Part 1. Results from direct numerical simulation," New J. Phys. **10**, 075015 (2008).
[33] L.-P. Wang, A. Wexler, and Y. Zhou, "Statistical mechanical description and modelling of turbulent collision of inertial particles," J. Fluid Mech. **415**, 117 (2000).
[34] J. P. L. Salazar and L. R. Collins, "Inertial particle relative velocity statistics in homogeneous isotropic turbulence," J. Fluid Mech. **696**, 45 (2012).
[35] K. Gustavsson, S. Vajedi, and B. Mehlig, "Clustering of particles falling in a turbulent flow," Phys. Rev. Lett. **112**, 214501 (2014).
[36] J. Davila and J. C. R. Hunt, "Settling of small particles near vortices in turbulence," J. Fluid Mech. **440**, 117-145 (2001).
[37] Y. Zhou, A. S. Wexler, and L. P. Wang, "Modelling turbulent collision of bidisperse inertial particles," J. Fluid Mech. **433**, 77-104 (2001).
[38] L.-P. Wang, O. Ayala, Y. Xue, and W. W. Grabowski, "Comments on droplets to drops by turbulent coagulation?," J. Atmos. Sci. **63**, 2397-2401 (2006).
[39] L.-P. Wang, O. Ayala, and W. W. Grabowski, "On improved formulations of the superposition method," J. Atmos. Sci. **62**, 1255-1266 (2005).
[40] C. N. Franklin, P. A. Vaillancourt, M. K. Yau, and P. Bartello, "Collision rates of cloud droplets in turbulent flow," J. Atmos. Sci. **62**, 2451-2466 (2005).
[41] M. R. Maxey, "The motion of small spherical-particles in a cellular-flow field," Phys. Fluids **30**, 27 (1987).
[42] J. Chun, D. L. Koch, S. L. Rani, A. Ahluwalia, and L. R. Collins, "Clustering of aerosol particles in isotropic turbulence," J. Fluid Mech. **536**, 219-251 (2005).
[43] J. Ferry, S. L. Rani, and S. Balachandar, "A locally implicit improvement of the equilibrium Eulerian method," Int. J. Multiphase Flow **29**, 869-891 (2003).
[44] S. Balachandar and J. K. Eaton, "Turbulent dispersed multiphase flow," Annu. Rev. Fluid Mech. **42**, 111-133 (2010).